Differential Mobility of Skeletal and Cardiac Tropomyosin on the Surface of F-Actin†

Iype K. Chandy, Jun-Chih Lo, and Richard D. Ludescher*

Department of Food Science, Rutgers, The State University, 65 Dudley Road, New Brunswick, New Jersey 08901-8520

Received December 30, 1998; Revised Manuscript Received April 13, 1999

ABSTRACT: Polarized phosphorescence from the triplet probe erythrosin-5-iodoacetamide attached to sulfhydryls in rabbit skeletal and cardiac muscle tropomyosin (Tm) was used to measure the microsecond rotational dynamics of these tropomyosins in a complex with F-actin. The steady-state phosphorescence anisotropy of skeletal tropomyosin on F-actin was 0.025 ± 0.005 at 20 °C; the comparable anisotropy for cardiac tropomyosin was 0.010 ± 0.003. Measurements of the anisotropy as a function of temperature and solution viscosity (modulated by addition of glycerol) indicated that both skeletal and cardiac tropomyosin undergo complex rotational motions on the surface of F-actin. Models assuming either long axis rotation of a rigid rod or torsional twisting of a flexible rod adequately fit these data; both analyses indicated that cardiac Tm is more mobile than skeletal Tm and that the increased mobility on the surface of F-actin reflected either the rotational motion of a smaller physical unit or the torsional twisting of a less rigid molecule. The binding of myosin heads (S1) to the Tm−F-actin complexes increased the anisotropy to 0.049 ± 0.004 for skeletal and 0.054 ± 0.007 for cardiac tropomyosin. The titration of the skeletal tropomyosin−F-actin complex by S1 showed a break at an S1/actin ratio of 0.14; this complex had an anisotropy of 0.040 ± 0.007, suggesting that one bound head effectively restricted the motion of each skeletal tropomyosin. A similar titration with cardiac tropomyosin reached a plateau at an S1/actin ratio of 0.4, suggesting that 2−3 myosin heads are required to immobilize cardiac Tm. Surface mobility is predicted by structural models of the interaction of tropomyosin with the actin filament while the decrease in tropomyosin mobility upon S1 binding is consistent with current theories for the proposed role of myosin binding in the mechanism of tropomyosin-based regulation of muscle contraction.

Molecular models of the regulation of force generation are now animated in considerable structural detail. The thin filament regulatory proteins tropomyosin (Tm)[1] and troponin form an elongated complex polymerized along the long-pitch helix of the actin filament. Each tropomyosin, a ∼41 nm long, dimeric, α-helical coiled-coil, forms the backbone of the complex and binds to seven actin monomers. In regulated thin filaments, tropomyosin binds in different positions depending upon whether Ca^{2+} is present (*1, 2*); this provides independent evidence for the original steric blocking model of regulation (*3*−*5*). The steric blocking model proposes that tropomyosin regulates actomyosin interactions by switching between an "off" state in which Tm sterically blocks myosin binding sites on actin and an "on" state in which it does not. Ca^{2+} binding to Troponin C is postulated to switch tropomyosin from the off to the on state, thus preparing the filament for myosin binding and subsequent force generation.

Studies of actomyosin interactions in solution, however, have long emphasized the primary role that the binding of myosin heads play in switching the filament from the off to the on state. In the absence of troponin, the actin-activated ATPase activity is inhibited by tropomyosin at low S1 and activated at high S1 concentrations (*6*); the actin-activated ATPase activity is thus cooperative in the presence of tropomyosin. More recently, studies of actoS1 interaction kinetics provide evidence for three states of the regulated thin filament: a blocked state which cannot bind S1, a closed (off) state that binds S1 weakly, and an open (on) state that binds S1 strongly (*7, 8*). S1 (and thus myosin) binds to F-actin in a two step process: weak binding in the so-called "A" or attached state followed by isomerization to a strong binding ("R" or rigor) state (*9*). The presence and state of the nucleotide on myosin determines the equilibrium between A and R states: ATP and ADP + Pi binding favor weak A state binding while ADP or no nucleotide favor strong R state binding (*10, 11*); only heads bound in the R state can generate force.

A recent model postulates that regulation is controlled by three distinct binary equilibria involving tropomyosin, troponin, and myosin (*12*): tropomyosin fluctuating between off and on states, troponin switching between "blocked" and "closed" states, and myosin isomerizing between A and R states. The fluctuations of tropomyosin between two different

† This research was supported by a grant from the Muscular Dystrophy Association (to R.D.L.) and a Graduate Fellowship from the American Heart Association−New Jersey Affiliate (to I.K.C.). Publication no. D-10567-1-99 of the New Jersey Agricultural Experiment Station.

* To whom correspondence should be addressed. Fax: 732-932-6776. Phone: 732-932-9611 ext. 231. E-mail: ludescher@aesop.rutgers.edu.

[1] Abbreviations: DTT, dithiothreitol; EPPS, 4-(2-hydroxyethyl)-1-piperazine ethanesulfonic acid; Er5IA, erythrosin-5-iodoacetamide; Mops, 4-morpholine propanesulfonic acid; SBW, spectral bandwidth; S1, myosin subfragment 1; Tm, tropomyosin; TnC, troponin C; TnI, troponin I; TnT, troponin T; Tris-HCl, 2-amino-2-hydroxymethyl-1,3-propanediol.

10.1021/bi983073s CCC: $18.00
Published on Web 07/02/1999

positions on the actin surface are thought to occur both in the absence and in the presence of Ca^{2+}; calcium only acts as an allosteric effector to shift the equilibrium toward the on state. Calcium acts as a switch, however, to shift the troponin complex from a blocked state to one in which the inhibition is removed (closed state). Calcium thus activates the filament both by switching Tn to the closed state and by shifting the Tm equilibrium to the on state. Myosin heads can only bind to the closed state and can only isomerize from the weak binding A to the force generating R state when Tm is on.

Although this model for force regulation is thought to apply to all striated muscles, subtle differences in the composition of tropomyosin may modulate some of the details. Four tropomyosin genes have been identified; their products are designated α-Tm, *β*-Tm, *γ*-Tm, and *δ*-Tm (*13*). Skeletal muscle tropomyosin of rabbit (the animal source for these studies) is composed of a mixture of 4 α and 1 *β*-chains (*14*); cardiac tropomyosin, however, consists only of α-chains. Little is known, however, of the functional significance of the different isoforms. One study (*15*) noted that head-to-tail interactions between Tm molecules were greatest for *ββ*, lesser for α*β*, and less still for αα. This suggests that the presence of *β*-chains may modulate the motions and perhaps enhance the cooperativity of tropomyosin.

Conformational fluctuations of tropomyosin on the surface of F-actin thus play a crucial physical role in current models of regulation; myosin binding to F-actin and Ca^{2+} binding to troponin C are thought to modulate these fluctuations. We have initiated direct studies of the rotational motions of tropomyosin on the microsecond time scale using phosphorescence emission anisotropy of the triplet probe erythrosin-5-iodoacetamide covalently attached to sulfhydryls on skeletal and cardiac tropomyosin; preliminary results have been reported elsewhere (*16*−*19*). The complex nature of the microsecond rotational motions of tropomyosin in the complex with F-actin (but without troponin) was established by measurements of the effect of temperature and viscosity on the steady-state phosphorescence emission anisotropy of the probe. Analysis of these data using two different motional models (long axis rotation of a rigid rod or torsional twisting of a flexible rod) supports the conclusion that cardiac αα-Tm is more mobile than skeletal Tm containing 20% *β*-chains. The binding of myosin heads (S1) severely restricted the mobility of both skeletal and cardiac tropomyosin on the surface of F-actin, suggesting that this tropomyosin mobility is related to the physiological role of Tm in controlling the functioning of the thin filament.

MATERIALS AND METHODS

Protein Preparations. All proteins were isolated from acetone powder prepared from the leg and back muscles of New Zealand white rabbits. Procedures for isolation of cardiac and skeletal tropomyosin were the same. Tropomyosin was extracted into high-salt extraction buffer (1 M KCl, 0.5 mM DTT, pH 7.0) at room temperature. Subsequent procedures were carried out on ice or at 4 °C. The extracts were adjusted to pH 4.6 with 1 N acetic acid, stirred, and centrifuged at 6000*g*; the precipitate was dissolved in extraction buffer, and insoluble material was removed by centrifugation. Precipitation and dissolution were repeated twice more, and the final pH 4.6 precipitate was dissolved in 0.5 mM DTT (pH 7.0). Solid ammonium sulfate was added to 53% saturation at pH 7.0, the precipitate removed by centrifugation, the supernatant brought to 65% saturation, and the resulting precipitated tropomyosin was collected by centrifugation at 11000*g*, dissolved in 0.5 mM DTT (pH 7.0), and dialyzed overnight against pH 7.0 buffer containing 2 mM 2-mercaptoethanol. The purified tropomyosin was freeze-dried and stored at −20 °C. Actin was extracted from acetone powder into G-buffer (1 mM EPPS, 0.2 mM $CaCl_2$, 1 mM NaN_3, and 0.2 mM ATP, pH 8.5) plus 0.5 mM DTT on ice with hand stirring as described (*20*). Analysis of purity by SDS−PAGE indicated that the preparations were free of any contaminating proteins. F-actin was stored by dialysis in F-buffer (10 mM Mops, 100 mM KCl, 2 mM $MgCl_2$, 0.2 mM $CaCl_2$, 1 mM NaN_3, and 0.2 mM ATP, pH 7.0) at 4 °C; the dialysis solution was changed weekly.

Labeling of Tropomyosin. Cardiac and skeletal tropomyosins were labeled in the same manner. Tropomyosin was dissolved at about 2 mg/mL in labeling buffer (150 mM KCl and 10 mM Tris-HCl, pH 8.0) supplemented with 5 mM DTT, dialyzed against the same buffer at 4 °C overnight, and then dialyzed against labeling buffer to remove DTT. Erythrosin-5-iodoacetamide (Molecular Probes, Eugene, OR) in *N*,*N*-dimethylformamide (10 mM stock) was added in 2.5-fold excess to the tropomyosin solution, and the reaction was allowed to continue for 4−12 h in the dark at 37 °C (longer labeling times gave higher extents of labeling). DTT was added to terminate the reaction. Labeling ratios in excess of 1 dye/tropomyosin dimer were achieved by adding either excess dye (up to 7.5-fold molar excess) or by labeling for longer times (up to 72 h). The labeled tropomyosin was dialyzed overnight against excess high-salt buffer (1 M KCl and 20 mM Mops, pH 7.0) supplemented with 0.1 mg/mL bovine serum albumin. The residual unreacted probe was removed by gel filtration through a 1.5 × 15 cm column of Sephadex G-25 in high-salt buffer (erythrosin binds noncovalently to this gel). Greater care was taken with the samples labeled at higher dye/protein ratios to ensure complete removal of unreacted dye (a 1.5 × 27 cm Sephadex G-25 column, for example). The labeled tropomyosin was freeze-dried and stored at −20 °C.

The extent of labeling was determined by dissolving labeled tropomyosin at about 1 mg/mL in high-salt buffer, diluting to an appropriate concentration, and measuring the absorbance at 600, 530, 320, and 277 nm. The concentration of erythrosin was calculated using $[Er5IA] = (A_{530} - A_{600})/83000$. The concentration of tropomyosin was calculated using $[Tm] = \{A_{277} - [Er5IA]16000 - (A_{320} - [Er5IA]6500)\}/22000$. The extinction coefficients for erythrosin-5-iodoacetamide at 530, 320, and 277 nm are 83 000, 6500, and 16 000 M^{-1} cm^{-1}, respectively (erythrosin does not absorb at 600 nm); the extinction coefficient of tropomyosin at 277 nm is 22 000 M^{-1} cm^{-1} (based on an extinction coefficient of 0.33 $(mg/mL)^{-1}$ cm^{-1} and a molecular weight of 66 000 for the Tm dimer). The extent of labeling ([Er5IA]/[Tm] or dye/protein) for the labeled tropomyosin was in the range 0.4−1.1 for skeletal and 0.7−0.9 for cardiac tropomyosin, unless noted otherwise.

Preparation of Actin−*Tropomyosin Complex.* The F-actin−tropomyosin complex was prepared by mixing labeled

tropomyosin and F-actin at a molar ratio of 1:7 (Tm:G-actin) and dialyzing the mixture against F-buffer plus 0.5 mM DTT at 4 °C overnight. The mixture was centrifuged at 200000*g* for 1.5 h at 4 °C to collect the complex. The pellet was carefully dispersed in the same buffer with a Dounce homogenizer, and the complex was dialyzed against F-buffer at 4 °C until used. The fraction of free tropomyosin in the Tm−F-actin samples under spectroscopic conditions was estimated by centrifugation. Samples of a labeled-Tm−F-actin complex at a total protein concentration equivalent to that used in phosphorescence anisotropy measurements were centrifuged in a Beckman TL100 tabletop ultracentrifuge using a TLA-100 rotor at 60 000 rpm (157 000 g) for 25 min. Samples of the pellets, supernatants, and uncentrifuged controls were immediately run on SDS−PAGE, stained, and the bands scanned using a Computing Densitometer model 300A; the band intensities were quantified using ImageQuant software.

Spectroscopic Measurements. All fluorescence measurements were made using a SPEX Industries (Metuchen, NJ) model F1T11i spectrofluorometer. Fluorescence intensity studies of labeled tropomyosin used an excitation wavelength of 480 nm (3.8 nm spectral bandwidth); the emission wavelength was typically 500−650 nm (3.8 nm SBW). Fluorescence anisotropy measurements were made over the emission band from 530 to 620 nm (3.8 nm SBW) using an excitation wavelength of 480 nm (15 nm SBW). Polarization intensities were measured using Glan−Thompson crystal polarizers in both the excitation and emission light paths. Intensities were measured using vertical and horizontal polarization in both excitation and emission. The polarization anisotropy was calculated using the following relation: $r = (R - 1)/(R + 2)$, where $R = (I_{vv}/I_{vh})(I_{hh}/I_{hv})$; the polarized intensities I_{ij} refer to the intensity with excitation polarization i and emission polarization j. Background signal was subtracted from the individual I_{ij} components where appropriate.

Phosphorescence measurements were made on the same instrument equipped with a model 1934D phosphorimeter attachment (SPEX Industries, Metuchen, NJ) consisting of a low pressure Xe flash lamp and a gated delay generator. In delayed emission (phosphorescence) spectral scans, the excitation wavelength was 480 nm (30 nm SBW) and the emission wavelength was in the range 500−850 nm (7.5 nm SBW); intensities were collected using an initial time delay of 0.07 ms and a time window of 1 ms. Phosphorescence intensity decays were collected over a time window of typically 1.5 ms using an initial time delay of 0.07 ms and time increments of 0.01 ms; excitation was at the peak of the excitation spectrum at 534 nm (30 nm SBW) and the emission was at 690 nm (30 nm SBW). Phosphorescence anisotropy measurements were made in the steady-state mode using 532 nm excitation (30 nm SBW) and 685 nm emission (30 nm SBW) and collecting intensity over a time window of 1.5 ms following an initial delay of 0.07 ms. All phosphorescence measurements were made on samples deoxygenated using an enzyme system consisting of glucose (0.3% w/v), glucose oxidase (0.002 mg/mL), and catalase (0.02 mg/mL); the headspace above the liquid in the cuvette was also purged with argon during the experiments.

Phosphorescence intensity decays were analyzed using the program NFIT (Island Products, Galveston, TX), which employs a nonlinear least-squares iterative fitting procedure using the Marquardt−Levenberg algorithm to minimize deviations of the fit functions from the data. Decay curves were fit to single-exponential decay functions, and the lifetime reported is the time constant for this decay; typical fits had χ^2 values in the range 1.2−1.5, indicating that the single-exponential decay provided a satisfactory approximation of the intensity decay.

Analysis of Steady-State Phosphorescence Emission Anisotropy Data. For isotropic, unrestricted rotation of a probe rigidly attached to a spherical protein, the steady-state phosphorescence anisotropy (r_p) is given by

$$r_p = r_o/(1 + \tau/\phi) \quad (1)$$

[r_o is the intrinsic anisotropy without rotational motion (equal to 0.21 for erythrosin on our instrument (*20*), τ is the phosphorescence lifetime, and ϕ is the rotational correlation time of the depolarizing motion.] The rotational correlation time of a sphere is given by

$$\phi = \eta V/k_B T \quad (2)$$

(η is the viscosity of the solution, V is the effective hydrodynamic volume of the spherical protein, k_B is the Boltzmann constant, and T is the absolute temperature.) It is possible to estimate the magnitude of V by measuring how changes in viscosity and/or temperature modulate the magnitude of the anisotropy; the analysis typically involves generation of a Perrin plot (*21*).

$$1/r_p = 1/r_o + (k_B/r_o V)(\tau T/\eta) \quad (3)$$

For simple isotropic motion, a plot of $1/r$ versus $\tau T/\eta$ (a modified Perrin plot) is linear and the slope is $k_B/r_o V$. Since r_o can be estimated from the extrapolation to zero $\tau T/\eta$, V can be easily calculated. In more complex situations, however, the Perrin plot will display curvature. In the case of complex rotational motion of a flexible or asymmetric protein, the Perrin plot will display downward curvature (*42*); if the protein changes conformation (denatures, for example) due to the effects of temperature, however, the Perrin plot may display upward curvature.

Tropomyosin is a coiled-coil with a long axis of 41 nm and a radius of about 0.87 nm (the radius of a circle equivalent to the 2.0 × 1.5 nm cross-sectional area of tropomyosin) (*26*, *27*). Interactions between the N- and C-termini of the molecule are expected to increase its effective length when polymerized on F-actin. The anisotropy averaged over the approximately 210 μs excited-state lifetime of erythrosin is expected to reflect large-scale rotational motions about the long axis of this remarkably asymmetric molecule. There are two different models available to interpret the anisotropic depolarization that results from these long axis rotations: rotation about the long axis of a rigid cylinder and torsional twisting about the long axis of a flexible cylinder.

The emission anisotropy decay of a rigid asymmetric molecule with rodlike symmetric (equivalent to that of a prolate ellipsoid) has three components (*24*):

$$r(t) = r_1 \exp[-(D_{\|} + 5D_{\perp})t] + r_2 \exp[-(4D_{\|} + D_{\perp})t] + r_3 \exp[-(6D_{\perp})t] \quad (4)$$

where $D_{||}$ is the diffusion coefficient for rotation about the long axis and $D_{\perp}$ is the diffusion coefficient for rotation about the short axis of the molecule. These diffusion coefficients are related to the radius (b) and length (h) of the molecule:

$$D_{||} = k_B T/4\pi b^2 h\eta$$

$$D_{\perp} = (3k_B T/\pi h^3 \eta)[\ln(h/b) - \sigma] \quad (5)$$

where k_B is the Boltzmann constant, η is the solution viscosity, T is absolute temperature, and σ is also related to the asymmetry of the molecule:

$$\sigma = 1.57 - 7[1/\ln(h/b) - 0.28]$$

For an isolated tropomyosin molecule, the ratio of $D_{||}/D_{\perp} = 0.18(h/b)^2 = 406$ (using $h = 41$ nm and $b = 0.87$ nm); this ratio would be considerably larger for a polymerized tropomyosin molecule. We are thus justified in ignoring rotation about the short axis of tropomyosin and simplifying eq 4 to the following:

$$r(t) = r_1 \exp[-(D_{||})t] + r_2 \exp[-(4D_{||})t] + r_3 \quad (6)$$

The steady-state anisotropy for such a decay model (calculated from the intensity-weighted average of the anisotropy decay integrated from zero to infinity and using a single-exponential lifetime (τ) for the intensity decay) is

$$r_p = r_1/(1 + D_{||}\tau) + r_2/(1 + 4D_{||}\tau) + r_3 \quad (7)$$

Substituting for $D_{||}$ in eq 7, we generate the following expression for the steady-state anisotropy as a function of the viscosity ratio $\tau T/\eta$

$$r_p = r_1/(1 + k_B\tau T/4V\eta) + r_2/(1 + k_B\tau T/V\eta) + r_3 \quad (8)$$

In this expression, V is equal to the effective volume of tropomyosin ($V = \pi b^2 h$). Curves of r_p versus $\tau T/\eta$ were fit to eq 8 using V and the r_i terms as adjustable parameters using the program TableCurve 2D. Given the possibility that the rotational motion about the long axis is of limited amplitude, no effort was made to fit the r_i terms to the angles that the absorption and emission dipoles make with the long axis of the molecule (*24*).

The optical anisotropy of rodlike molecules such as DNA, F-actin, and perhaps tropomyosin, is best fit by a motional model involving torsional twisting about the long axis of the molecule within a restoring potential (*22*−*24*). The steady-state anisotropy corresponding to such torsional twisting motion is expressed as follows (*25*):

$$r_p = r_1 f(\tau/\Phi) + r_2 f(\tau/16\Phi) + r_3 \quad (9)$$

The function $f(\tau/\Phi)$ is a complex function of the ratio of the lifetime to the torsional twisting time Φ (*25*). The characteristic time for twisting is expressed as follows:

$$\Phi = \eta C(\pi b)^2/4(k_B T)^2 \quad (10)$$

where C is the torsional rigidity and b the radius of the rodlike molecule. The function $f(\tau/\Phi)$ is thus a function of the ratio $\tau T^2/\eta$. Curves of r_p versus $\tau T^2/\eta$ were fit to an explicit version of eq 9 using C and the r_i terms as adjustable parameters (*25*).

RESULTS

Spectroscopic Characterization of Erythrosin-Labeled Tropomyosin. The luminescence excitation and emission spectra of skeletal and cardiac tropomyosin labeled with erythrosin-5-iodoacetamide in a complex with F-actin were essentially identical (data not shown). The fluorescence emission maximum of 552 nm was unaffected by complex formation and the delayed emission spectra showed a smaller peak at shorter wavelengths due to delayed, E-type singlet emission (*28*) and a larger peak at longer wavelengths (~682 nm) due to triplet emission. The phosphorescence decays in F-buffer of the labeled Tm−F-actin complexes were well fit with single phosphorescence lifetimes of 0.213 ms for skeletal and 0.205 ms for cardiac Tm. The similar spectroscopic behavior of erythrosin on the two isoforms provides evidence for similar probe/protein interactions in skeletal and cardiac tropomyosin.

On the short time scale of the fluorescence lifetime of erythrosin, less than 1 ns (*29*), the steady-state fluorescence emission anisotropy (r_f) provides an estimate of probe motion only (*21*). The r_f in F-buffer of labeled skeletal tropomyosin alone and in a complex with F-actin were 0.28 and 0.26, respectively (the maximum value of r_f for the erythrosin in our instrument is 0.385 (*20*).) The phosphorescence anisotropy (r_p) of erythrosin-labeled skeletal tropomyosin was 0.025 ± 0.004 in the F-actin complex at 20 °C. This anisotropy was independent of the extent of labeling over the range 0.4−1.2 dye per skeletal tropomyosin dimer; the average anisotropy was 0.025 ± 0.005 for samples labeled at a dye/protein of 0.4−0.7, 0.027 ± 0.002 at dye/protein of 0.7−0.9, and 0.023 ± 0.007 for samples labeled at dye/protein of 0.95−1.2. The anisotropy of cardiac tropomyosin on F-actin labeled at dye/protein ratios of 0.7−0.9 was 0.010 ± 0.003 under the same conditions. (Labeled-tropomyosin alone, either skeletal or cardiac, in F-buffer, has an r_p of zero.) The lower cardiac anisotropy (r_p) was not due to differences in the extent of Tm bound in the two complexes; analysis by centrifugation indicated that 25 ± 10% of the labeled skeletal Tm versus 20 ± 9% of the labeled cardiac Tm was free of the complex (and thus contributing zero anisotropy); these unbound fractions are similar to that seen with pyrene-maleimide labeled Tm (*53*). Our measured values are thus slight underestimates of the average rotational motion of Tm in these complexes; corrected anisotropy values for the complexes are 0.033 (=0.025/0.75) for skeletal and 0.013 (=0.01/0.8) for cardiac Tm. Given the close similarity in the phosphorescence lifetimes, these data suggest that cardiac tropomyosin is more mobile than skeletal tropomyosin in the F-actin complex.

Effect of Temperature on the Phosphorescence Emission Anisotropy of Skeletal Tropomyosin. The phosphorescence emission anisotropy (r_p) in F-buffer of labeled skeletal tropomyosin in a complex with F-actin decreased monotonically over the temperature range 0−50 °C (Figure 1); the phosphorescence lifetime also decreased monotonically with temperature. The data in Figure 1 were used to generate a modified Perrin plot in which $1/r_p$ was plotted versus $\tau T/\eta$ (Figure 2). For simple rotational diffusive motion, this plot

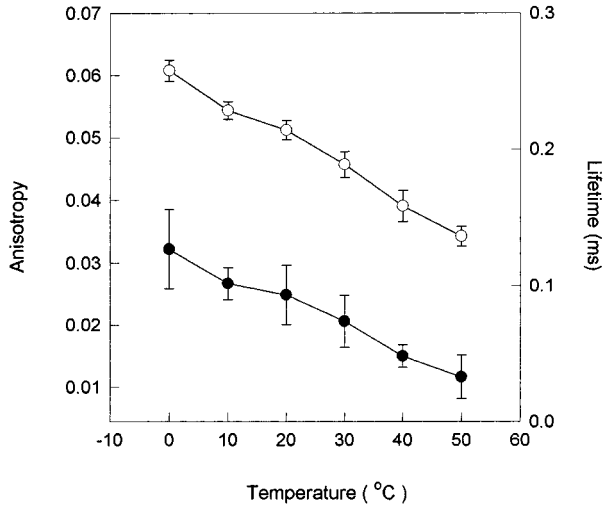

FIGURE 1: Phosphorescence emission anisotropy (●) and lifetime (○) of erythrosin-labeled skeletal tropomyosin in a complex with F-actin in F-buffer measured as a function of temperature. The averages of multiple measurements are plotted with the standard deviations indicated by the error bars.

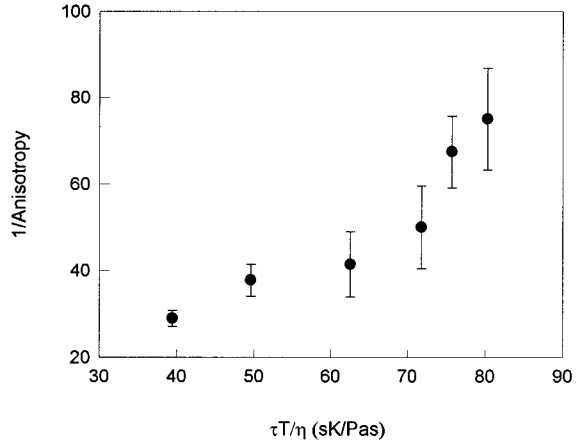

FIGURE 2: The effect of temperature on the phosphorescence emission anisotropy of erythrosin-labeled skeletal tropomyosin in a complex with F-actin in F-buffer. The anisotropy and lifetime data of Figure 2 were combined into modified Perrin plot (see Materials and Methods).

is linear with a slope equal to k_B/r_oV (see eq 3, Materials and Methods). The upward curvature at high $\tau T/\eta$ indicates that at 40 °C and above the anisotropy decreased more than would be expected due to the effect of temperature (and viscosity) on the rotational correlation time, suggesting a change in the structure of the complex. A decrease in the anisotropy could result from a decrease in the interactions between F-actin and tropomyosin (*30*) or from thermal unfolding of tropomyosin (*31*) that leads to an increase in rotational motion.

Effect of Viscosity on the Phosphorescence Emission Anisotropy of Tropomyosin. In an effort to characterize the motions that depolarize the phosphorescence anisotropy of labeled tropomyosin, the effect of viscosity on the anisotropy of the Tm−F-actin complexes was measured. F-buffer was supplemented with glycerol over the range 0−84% (wt/wt) at 20 °C; the viscosity of these solutions ranged 0.001−0.084 Pa s (*32*). The phosphorescence lifetime of labeled skeletal tropomyosin increased from 0.213 ms at 0% glycerol to a nearly constant value of 0.360 ms at glycerol concentrations

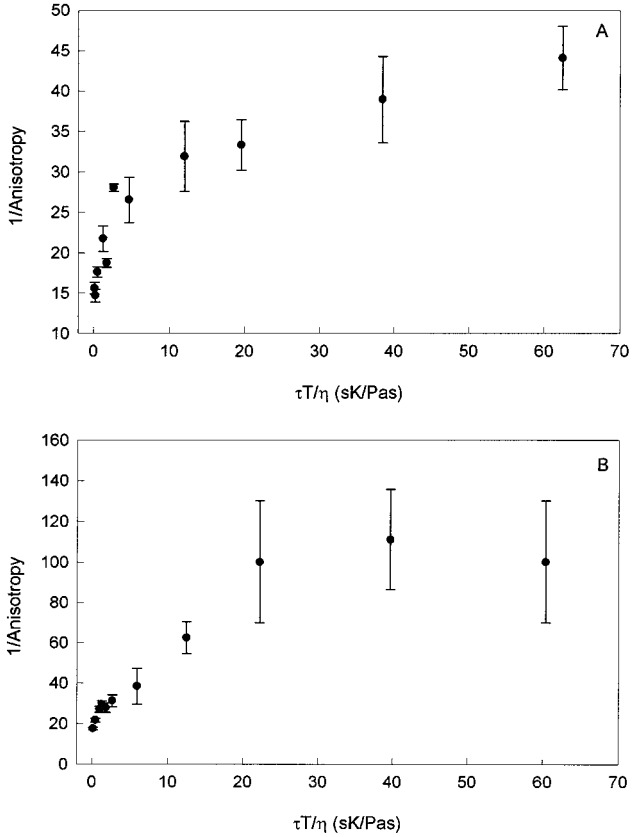

FIGURE 3: The effect of solution viscosity and temperature on the phosphorescence emission anisotropy of erythrosin-labeled skeletal (A) and cardiac (B) tropomyosin in a complex with F-actin. Solution viscosity was modulated by adding glycerol to a solution at 20 °C and by decreasing the temperature of an 80 wt % glycerol solution (see text for details). Data were plotted using a modified Perrin equation (see Materials and Methods).

of 68% and higher; similar trends were seen in the lifetime of erythrosin-labeled cardiac tropomyosin. The anisotropy was measured at higher solution viscosity by decreasing the temperature of F-buffer plus 80% (wt/wt) glycerol from 20 to −7 °C; these conditions vary the solution viscosity from 0.06 to 0.5 Pa s.

These variations in solution viscosity and temperature had a large influence on the anisotropy of both the skeletal (Figure 3A) and cardiac (Figure 3B) Tm−F-actin complexes. For skeletal Tm, the anisotropy increased from 0.025 at a viscosity of 0.001 Pa s (at 20 °C) to 0.064 at a viscosity of 0.5 Pa s (at −7 °C); over the same change in solution conditions the anisotropy of the cardiac Tm complex increased from 0.01 to 0.057. The downward curvature in the modified Perrin plots (Figure 3) suggests the presence of complex rotational motions depolarizing the anisotropy (*38*). In addition, such large changes in the anisotropy indicate that the time constants for these motions are increased by the change in viscosity to time scales comparable to the phosphorescence lifetime (∼0.21 ms). These r_p data were fit to two different motional models: long axis rotation of a rigid molecule and torsional twisting of a flexible molecule. In these analyses, the anisotropy data as a function of either $\tau T/\eta$ or $\tau T^2/\eta$ were fit to model functions as described in Materials and Methods.

In the long axis rotation model, a single, rigid rotating volume element characterizes the anisotropy versus viscosity

Table 1: Model Fit Parameters for the Anisotropy of Tropomyosin on F-Actin[a]

model	tropomyosin	amplitudes r_1	r_2	r_3	r_0[b]	V (nm^3)	torsional rigidity (N m^2)	rotation time[c] (μs)	goodness of fit[d]
long axis rotation	skeletal	0.033	0.018	0.023	0.074	8,440		2.1	0.942
	cardiac	0.035	0.029	0.003	0.067	4,850		1.2	0.984
torsional twisting	skeletal	0.049	0.014	0.020	0.083		2.1×10^{-26}	2.3	0.942
	cardiac	0.025	0.045	0.0035	0.074		0.76×10^{-26}	0.82	0.980

[a] Steady-state anisotropy data collected as a function of solution viscosity and temperature were fit to either a long axis rigid body rotation model (eq 8; Materials and Methods) or a flexible rod torsional twisting model (eq 9). [b] Equal to $r_1 + r_2 + r_3$. [c] Equivalent rotational times calculated in water at 25 °C; for the long axis rotation model, $\varphi = 1/D_{\parallel}$ (see eq 5, Materials and Methods) and for the torsional twisting model, Φ was calculated using eq 10 (Materials and Methods). [d] Statistical R^2 parameter for fit using the tabulated parameters.

data. The fit volumes for this model were 8.4×10^3 nm^3 for skeletal and 4.85×10^3 nm^3 for cardiac Tm (Table 1). The results from a fit to a torsional twisting motional model are also listed in Table 1. In this model, the anisotropy is modulated by the torsional rigidity of a flexible rod. Using a radius for tropomyosin of 0.87 nm (see Materials and Methods), this analysis suggested that the torsional rigidity of tropomyosin on F-actin was 2.1×10^{-26} N m^2 for skeletal and 0.76×10^{-26} N m^2 for cardiac Tm, respectively. The statistical quality of the data fits using the two models were equivalent (R^2 values were 0.942 and 0.942 for skeletal and 0.984 and 0.980 for cardiac data for the long axis and torsional twisting models, respectively).

The measured anisotropy and the results of the model analyses indicate that cardiac tropomyosin is more mobile on the surface of F-actin and that the increase in mobility is due either to a smaller effective volume of the rotating unit or to a lower torsional rigidity; either situation will give rise to a lower characteristic rotation time for the cardiac isoform (Table 1). The model analyses also provide an estimate of the effective r_o (equal to the sum of the fit amplitudes) for the anisotropy of erythrosin-labeled Tm in the F-actin complex (Table 1). The effective r_o provides an estimate of the anisotropy in the absence of the microsecond motions modulated by these changes in viscosity. The average value from the two models is about 0.078 for skeletal and 0.070 for cardiac Tm. These r_o values are less than the r_o of 0.21 for erythrosin on our instrument (*20*); the difference must reflect motions of the probe and perhaps segmental motions of the protein that occur on the nanosecond time scale.

Effect of S1 Binding on Skeletal and Cardiac Tropomyosin Dynamics. The measured anisotropy of the skeletal tropomyosin−F-actin complex without added S1 was 0.025 ± 0.004 at 20 °C in F−buffer. Upon titration with S1, the anisotropy of tropomyosin in the complex increased to 0.049 ± 0.004 at a final S1:actin ratio of 1:1 (Figure 4A). This value was only slightly smaller than the effective r_o for skeletal Tm in the F-actin complex (0.078) and indicates that myosin binding significantly restricted the microsecond rotational motions of skeletal tropomyosin on the surface of F-actin. The anisotropy clearly increased nonlinearly with S1 concentration. The anisotropy of tropomyosin in the 1:7:: S1:actin complex (S1/actin = 0.14) was 0.040 ± 0.007, a value not significantly different from the anisotropy of the 1:1 complex (0.049 ± 0.004); in fact, the tropomyosin anisotropy at all S1/actin ratios above 0.14 were similar and the same within experimental error. The high value of the anisotropy in the 1:7 complex suggests that the binding of only one myosin head restricted the rotational motion of one skeletal tropomyosin molecule.

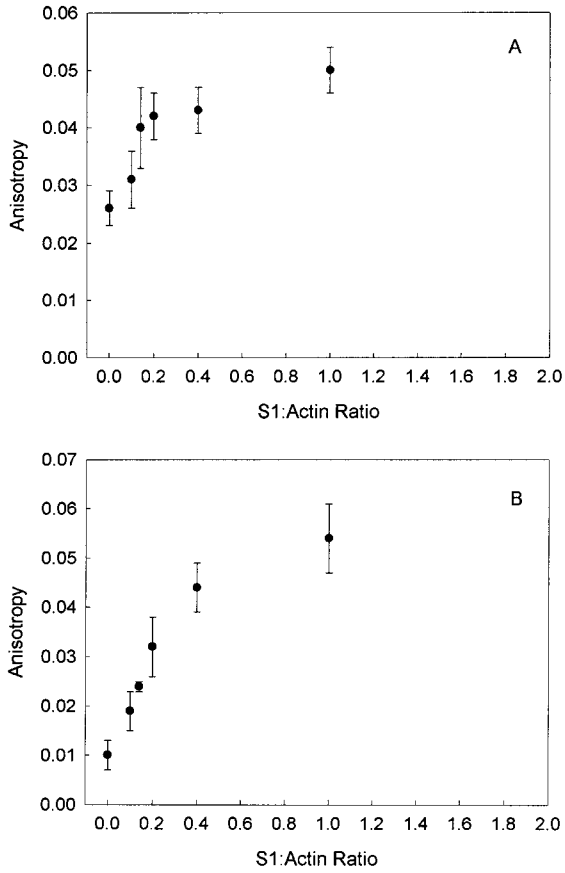

FIGURE 4: The effect of myosin head (S1) binding on the phosphorescence emission anisotropy of erythrosin-labeled tropomyosin in a complex with F-actin at 20 °C in F-buffer. The anisotropy (with standard deviations indicated) is plotted versus the molar ratio of S1/actin added to the solution. (A) Effect of S1 binding on anisotropy of skeletal tropomyosin. (B) Effect of S1 binding on anisotropy of cardiac tropomyosin.

The rotational dynamics of cardiac tropomyosin in a complex with F-actin were also restricted by S1 binding (Figure 4B). The measured anisotropy of the cardiac tropomyosin−F-actin complex increased from 0.010 ± 0.003 in the absence of S1 to 0.054 ± 0.007 at an S1:actin ratio of 1:1. Since the plateau value was similar to the effective r_o for cardiac Tm (0.070), S1 binding also significantly restricted the microsecond rotational motions of cardiac tropomyosin on F-actin. Interestingly, the final plateau value in the presence of S1 was larger for cardiac than for skeletal tropomyosin despite the significantly lower anisotropy of cardiac Tm in the absence of S1. The anisotropy increased in a nearly linear manner over the range 0.1−0.4 S1/actin ratio, with the anisotropy at an S1/actin ratio of 0.4 nearly identical to that at a ratio of 1. The rotational motion of

cardiac Tm thus appears to be effectively restricted when 2−3 myosin heads are bound per tropomyosin.

The average lifetime of the probe on skeletal Tm changed only slightly from its value without S1 bound (0.226 ms) over the entire course of the titration (values were 0.231, 0.234, 0.234, 0.225, and 0.224 ms for complexes with S1/actin ratios of 0.1, 0.14, 0.2, 0.4, and 1, respectively). Similar behavior was seen in the lifetime of labeled cardiac Tm during titration with S1 (lifetime of 0.205 ms in the absence and lifetimes of 0.227, 0.233, 0.232, 0.242, and 0.243 ms for complexes with S1/actin ratios of 0.1, 0.14, 0.2, 0.4, and 1, respectively). This near constancy of lifetime provided strong presumptive evidence that the increase in the anisotropy reflected decreases in the rate and/or amplitude of tropomyosin motion on the surface of F-actin resulting from S1 binding. (The slight increase, about 18%, seen in the cardiac Tm lifetime would actually cause a decrease in the anisotropy, all else remaining equal, rather than the increase measured.)

DISCUSSION

Influence of Multiple Labeling Sites in Skeletal Tropomyosin. Skeletal tropomyosin consists of α- and β-chains at a mole ratio of about 4:1 (*14*); cardiac tropomyosin consists only of α-chains. The α-chains from both skeletal and cardiac muscle contain a single sulfhydryl (Cys190) while the skeletal β-chain contains two sulfhydryls (Cys190 and Cys36) (*36*). Skeletal Tm thus contains a total of ∼2.4 potential sulfhydryl labeling sites, two sites on Cys190 in both α- and β-chains and ∼0.4 sites on Cys36 in the β-chain while cardiac Tm has only Cys190 sites in the α-chain. (Although iodoacetamide can react with unprotonated amines, this side reaction is negligible at pH 8 for two reasons. First, since the uprotonated amine is a weaker nucleophile than the unprotonated sulfhydryl (*39*), the reaction is slower. Second, at pH 8.0, the concentration of unprotonated sulfhydryl ($pK_a \approx 9-9.5$) is nearly 100-fold higher than the concentration of unprotonated amine ($pK_a \approx 10.5-11$). The N-terminus of Tm is acetylated and thus unreactive.) Although the anisotropy measurements of cardiac Tm reflect the perspective of a single probe at a single site (Cys190), this is probably not true for the skeletal molecule. Since Cys36 on β-Tm appears to be more reactive than Cys190 (*40, 41*), varying the labeling ratio over the range 0.4−1.2 will change the site of labeling from predominately Cys36 (at low ratios) to predominately Cys190 (at high ratios). If erythrosin-iodoacetamide reacts similarily to pyrene-iodoacetamide (*40, 41*), the distribution of label should vary from about 90% at Cys36 and 10% at Cys190 at a dye/protein of 0.4 to about 33% Cys36 and 67% Cys190 at a dye/protein of 1.2; a lower specificity for Cys36 will affect the distribution at each dye/protein but not the trend. Despite this change in probe distribution, the phosphorescence anisotropy was found to be constant over a 3-fold change in dye/protein from 0.4 to 1.2. The erythrosin anisotropy thus provided an average measure of the rotational motion of skeletal tropomyosin that was independent of the specific labeling site. A direct comparison of the anisotropy of skeletal and cardiac Tm is justified despite the differences in labeling sites.

Effect of Glycerol on Tropomyosin Dynamics. Several lines of evidence suggest that glycerol does not significantly modulate the structure of the Tm−F-actin complex. First, the modified Perrin plots of both skeletal and cardiac Tm−F-actin complexes display the typical downward curvature expected for the effect of viscosity on complex rotational motion (*38*) and not the upward curvature seen under conditions in which the structure of the complex is modified (Figure 2) or tropomyosin is dissociated. The anisotropy of the Tm−F-actin complex at 20 °C, for example, was essentially constant from 0 to 44% (w/w) glycerol for both isoforms (values of $\tau T/\eta$ in Figure 3 ranging 60−20 s K/Pa s). Even if glycerol were to promote Tm binding, however, this would only increase the anisotropy by 20−25%; given the large increases in anisotropy that glycerol induces (nearly 300% for skeletal and over 500% for cardiac) such an affect would not significantly influence the measured Perrin plots. Second, aqueous glycerol (50% v/v) is widely used to store myosin (*44*) and muscle fibers and myofibrils (*45*); the retention of calcium regulation in glycerinated myofibrils and fibers demonstrates that glycerol does not modulate thin filament structure or dissociate Tm. Third, aqueous glycerol (often in concentrations exceeding 65%) is widely used as a cryosolvent for studies of protein structure at low temperature (*33, 46, 47*) including a phosphorescence study of G- and F-actin in 60% glycerol (*48*). This is due to the ability of glycerol (and other polyols) to stabilize proteins (*49*−*51*). We are thus confident glycerol does not significantly perturb the Tm−F-actin complex and that any affect on Tm binding does not significantly affect our dynamic analysis.

Tropomyosin Rotational Motions on F-Actin. The microsecond motions of tropomyosin have been analyzed using two different motional models: long axis rotation of a rigid molecule and torsional twisting of a flexible molecule. It is not possible to distinguish between these models using statistical criteria. Despite this uncertainty, the results from the viscosity studies clearly indicate that cardiac Tm is more rotationally mobile than skeletal Tm on the surface of F-actin. The physical origin of the increased mobility of cardiac Tm, however, remains uncertain: either cardiac Tm has a smaller effective volume on the filament or cardiac Tm has a smaller torsional rigidity.

A model for the Tm−F-actin complex provides a molecular framework within which to discuss our results (*35*). This model places tropomyosin in closest contact with subdomains 3 and 4 of actin; interactions are mainly electrostatic since tropomyosin is about 1.0 nm from the nearest actin C^{α} carbons. A specific radial and azimuthal position of Tm is strongly preferred, suggesting that its position on the filament surface is relatively fixed in the absence of troponin and myosin. There is, however, considerable variability possible in the specific rotational orientation of tropomyosin. Electrostatic interactions between charged residues give rise to an electrostatic potential that varies from about −15 kcal/mol to +12 kcal/mol depending upon the rotational orientation of tropomyosin about its long axis (see Figure 8 of ref *35*). Rotations of about ±45° about the minimum position in the electrostatic potential appear reasonable.

On the basis of this model, we suggest that the phosphorescence anisotropy monitors long axis rotations of tropomyosin which occur within a diffuse electrostatic potential on the surface of F-actin. The model also provides a plausible explanation for the differences in rotational mobility between skeletal and cardiac Tm, which differ only in the presence

of the β-isoform in skeletal Tm [the α-chains of skeletal and cardiac Tm are identical (*36*)]. β-tropomyosin has the same number of residues as α-Tm but differs in sequence at 39 sites; although most of these substitutions are conservative (Asp for Glu, for example), two involve substitutions of charged for uncharged residues. Ser229 and His276 in skeletal (and cardiac) α-Tm become Glu229 and Asn276 in β-Tm. The result is that the overall charge of β-Tm is 1−2 units more negative (depending upon the pH and the pK_a of His276) than α-Tm. (The other changes in the C-terminal overlap region are conservative: Met281 and Iso284 become Iso281 and Leu284 in the β-chain). Lorenz and colleagues (*35*) have calculated that the favorable electrostatic interactions between Tm and actin contribute anywhere from −0.37 to −0.93 kcal/mol of charge interaction; a change in two of these interactions could thus change the electrostatic potential by 0.74−1.86 kcal/mol. Such a change in the angular potential could modulate the amplitude and/or rate of rotational motions of tropomyosin on F-actin, or change the torsional rigidity of tropomyosin by modulating the torsional potential. Detailed interpretation of the effects of the electrostatic angular potential on the rotational motions of tropomyosin, however, awaits more detailed theoretical modeling. Such a study must also explain how the rotational motion of tropomyosin is affected so dramatically by the presence of 20% β-chain. Part of the effect may be related to the thermodynamic preference of αβ- over αα- and $\beta\beta$-dimers, which means that 36% ($1-0.8^2$) of Tm molecules contain a β-chain. If these αβ-dimers are ramdomly distributed along the actin filament then there is about a 60% probability ($1-0.64^2$) that head-to-tail interactions involve an αβ-dimer.

The calculated volumes of the rotating elements of skeletal and cardiac Tm are 8.4×10^3 and 4.85×10^3 nm^3. Such volumes correspond to tropomyosin-sized filaments of lengths about 3.6 and 2.1 μm, corresponding to aggregates of about 94 skeletal and 54 cardiac Tm molecules. Since it is difficult to imagine how 54−94 tropomyosin molecules polymerized in a helical fashion about F-actin could move as a single rigid volume element, this elementary calculation seriously undermines the physical plausibility of the rigid rod physical model.

A torsional twisting model, on the other hand, generates a more plausible picture of the motion of tropomyosin on the surface of F-actin. This analysis indicates that tropomyosin is a flexible molecule with torsional rigidities of 2.1×10^{-26} N m^2 for skeletal and 0.76×10^{-26} N m^2 for cardiac Tm. The calculated rigidities for Tm are similar to those determined for F-actin. Yasuda et al. (*37*) determined from optical manipulation measurements that the rigidity of actin filaments was either 2.8×10^{-26} or 8.5×10^{-26} N m^2 depending upon whether Mg^{2+} or Ca^{2+}, respectively, was the tightly bound divalent cation (our measurements were of Tm on Ca^{2+}-F-actin). Time-resolved optical anisotropy studies, however, generated smaller rigidities of either 0.2×10^{-2} (*34*) or 0.14×10^{-26} N m^2 (*24*) for what were presumably Ca^{2+}-F-actin samples. The origin of these discrepancies is unclear and limits any detailed comparison with our measurements. Our measurements, however, would be the first estimates of the torsional rigidity of an α-helical coiled-coil molecule.

In the context of the more plausible torsional twisting model, the dynamic differences between skeletal and cardiac tropomyosin reflect an approximately 3-fold difference in the torsional rigidity of the molecules. As noted above, a more rigid skeletal molecule must reflect the presence of β-chains in this isoform. Whether the presence of the β-chain directly increases the intrinsic rigidity of the molecules or whether the increased rigidity reflects the effect of the β-chain on either the electrostatic interactions with the surface of F-actin or the head-to-tail interactions between polymerized Tm molecules (*43*) remains to be confirmed. Given the known structure of the Tm−F-actin complex and the recognition that torsional twisting dominates the motion of filamentous molecules such as F-actin and DNA, such a model, albeit not proven, remains the most plausible physical model for microsecond rotational motions of tropomyosin on F-actin.

Influence of Myosin Head Binding on Tropomyosin Dynamics. S1 binding increases the anisotropy of both skeletal and cardiac Tm on the surface of F-actin. This influence is dramatic for both isoforms, increasing the anisotropy by a factor of 2 for skeletal and a factor of 5 for cardiac tropomyosin with no concomitant changes in the probe lifetime. Although S1 is known to increase the affinity of unlabeled Tm for actin (*52*), such an effect would only increase the anisotropy of each isoform by 20−25% and thus cannot explain the large increases seen upon S1 binding. S1 binding must modulate the dynamics of tropomyosin by reducing either the rate or the extent of Tm rotational motions on the surface of F-actin. Within the context of the torsional twisting model, reducing the rate of motion would involve increasing the torsional rigidity of the protein. Limiting the extent of motion could result from direct physical interactions between myosin heads and Tm that limit the extent of molecular twisting; this is exactly the physical model depicted in current models of regulation (*7, 12*). Since the equilibrium position of Tm in the molecular model of the tropomyosin−F-actin complex (*35*) partially overlaps the myosin-binding site on actin, it is probable that S1 binding results in direct physical contacts between myosin heads and Tm. Such contacts could change the electrostatic potential within which Tm moves and, as pointed out by Lorenz and colleagues (*35*), could force Tm to adopt an alternate equilibrium position on the surface of F-actin. Such a change, of course, is required by imaging data (*4*) and a model in which S1 binding in the R state, that is, in the absence of nucleotide, constrains Tm to the on state *(7, 12*). Within the context of our findings about Tm motion on F-actin, Tm in the off state on the thin filament could be torsionally mobile (less rigid and thus able to twist rapidly or extensively about its long axis) while Tm in the on state could be torsionally immobile (more rigid and thus able to twist less rapidly or extensively about its long axis). In this view, troponin could manipulate the position of Tm on actin, and thus regulate actomyosin interactions, by modulating the torsional twisting motions of tropomyosin. Experiments to test this prediction are in the planning stages.

The effect of S1 binding on the anisotropy differs for skeletal and cardiac Tm. The binding of about 1 head/tropomyosin molecule (plateau at about 0.14 S1/actin) effectively restricts the rotations of skeletal Tm, a finding in agreement with previous results (*42*). The binding of 2−3

heads, however, are required to restrict the rotational motions of cardiac Tm (plateau at about 0.4 S1/actin). The physical origins of this difference are unclear but may reflect differences in the interactions between S1 and the two Tm isoforms or, perhaps, differences in their intrinsic torsional rigidity. If so, these differences must be significant to have an effect when only about one-third of the Tm molecules contains a β-chain.

Conclusions. Our studies suggest that both skeletal and cardiac tropomyosin move on the surface of F-actin on the microsecond time scale. Although either rotation of a rigid rod or torsional twisting of a flexible rod can satisfactorily describe the effect of viscosity on the anisotropy, consistency with previous studies and physical considerations lead us to conclude that these motions result from torsional twisting of a flexible Tm polymer on the surface of F-actin. The results of either analysis, however, clearly indicate that cardiac Tm is more mobile on the surface of F-actin than skeletal Tm. Given the significant restrictions in Tm motion that result from the binding of myosin heads (S1), the motions detected on the phosphorescence time scale appear to relate to the physiological role that tropomyosin plays in regulating force generation in striated muscle and agree, qualitatively at least, with the predictions of current models for force regulation in striated muscle (*12*). Expanding on a previous suggestion (*35*), we speculate that changes in the torsional rigidity of tropomyosin may play a specific role in the mechanism of force regulation in striated muscle.

REFERENCES

1. Wakabayashi, T., Huxley, H. E., Amos, L. A., and Klug, A. (1975) *J. Mol. Biol. 93*, 477−497.
2. Lehman, W. Craig, R., and Vibert, P. (1994) *Nature 368*, 65−67.
3. Haselgrove, J. C. (1972) *Cold Spring Harbor Symp. Quantum Biol. 37*, 341−352.
4. Huxley, H. E. (1972) *Cold Spring Harbor Symp. Quantum Biol. 37*, 361−376.
5. Parry, D. A. D., and Squire, J. M. (1973) *J. Mol. Biol. 75*, 33−55.
6. Lehrer, S. S., and Morris, E. P. (1982) *J. Biol. Chem. 257*, 8073−8080.
7. McKillop, D. F. A., and Geeves, M. A. (1994) *Biophys. J. 65*, 693−701.
8. Geeves, M. A., and Conibear, P. B. (1995) *Biophys. J. 68*, 194s−201s.
9. Coates, J. H., Criddle, A. H., and Geeves, M. A. (1985) *Biochem. J. 232*, 351−356.
10. McKillop, D. F. A., and Geeves, M. A. (1991) *Biochem. J. 279*, 711−718.
11. Geeves, M. A. (1991) *Biochem. J. 274*, 1−14.
12. Lehrer, S. S. (1994) *J. Musc. Res. Cell Motil. 15*, 232−236.
13. Smillie, L. B. (1998) *Guidebook to the Cytoskeleton and Motor Proteins*, Oxford University Press, Oxford.
14. Cummins, P., and Perry, S. V. (1973) *Biochem. J. 133*, 765−777.
15. Thomas, L., and Smillie, L. B. (1994) *Biophys. J. 66*, A310.
16. Lo, J.-C., and Ludescher, R. D. (1994) in *Time-Resolved Laser Spectroscopy in Biochemistry IV* (Lakowicz, J. R., Ed.) Vol. 2137, pp 494−502, SPIE Proceedings Series, Bellingham, WA.
17. Lo, J.-C., and Ludescher, R. D. (1995) *Biophys. J. 68*, A285.
18. Chandy, I. K., and Ludescher, R. D. (1996) *Biophys. J. 70*, A49.
19. Chandy, I. K., and Ludescher, R. D. (1999) *Biophys. J. 76*, A280.
20. Ludescher, R. D., and Liu, Z. (1994) *Photochem. Photobiol. 58*, 858−866.
21. Lakowicz, J. R. (1983) *Principles of Fluorescence Spectroscopy*, Plenun Press, New York.
22. Schurr, J. M. (1984) *Chem. Phys. 84*, 71−96.
23. Yoshimura, H., Nishio, T., Mihashi, K., Kinosita, K., and Ikegami, A. (1984) *J. Mol. Biol. 179*, 453.
24. Prochniewicz, E., Zhang, Q, Howard, E. C., and Thomas, D. D. (1996) *J. Mol. Biol. 255*, 446−457.
25. Ludescher, R. D., and Ludescher, W. H. (1993) *Photochem. Photobiol. 58*, 881−883.
26. Phillips, G. N., Lattman, E. E., Cummins, P., Lee, K. Y., and Cohen, C. (1979) *Nature 278*, 413−417.
27. Phillips, G. N., Fillers, J. P., and Cohen, C. (1986) *J. Mol. Biol. 192*, 111−131.
28. Garland, P. B., and Moore, C. H. (1979) *Biochem. J. 183*, 561−572.
29. Ludescher, R. D. (1990) *Spectroscopy 5*, 20−31.
30. Tanaka, H., and Oosawa, F. (1971) *Biochim. Biophys. Acta 253*, 274−283.
31. Woods, F. (1969) *Int. J. Protein Res. 1*, 29−43.
32. Weast, R. C., Ed. (1971) *Handbook of Chemistry and Physics*, 51st ed., The Chemical Rubber Co., Cleveland, OH.
33. Mak. A. H. (1995) *Methods Enzymol. 246*, 610−638.
34. Yoshimura, H., Nishio, T., Mihashi, K., Kinosita, K., and Ikegami, A. (1984) *J. Mol. Biol. 179*, 453−467.
35. Lorenz, M., Poole, K. J. V., Popp, D., Rosenbaum, G., and Holmes, K. C. (1995) *J. Mol. Biol. 246*, 108−119.
36. Mak, A. S., Lewis, W. G., and Smillie, L. B. (1979) *FEBS Lett. 105*, 232−234.
37. Yasuda, R., Miyata, H., And Kinosita, K., Jr. (1996) *J. Mol. Biol. 263*, 227−236.
38. Lakowicz, J. R., Maliwal, B., Cherek, H., and Balter, A. (1983) *Biochemistry 22*, 1741−1752.
39. Lundblad, R. L., and Noyes, C. M. (1984) *Chemical Reagents for Protein Modification*, Vol. I, CRC Press, Boca Raton, FL.
40. Lin, T. I. (1982) *Biophys. Chem. 15*, 277−288.
41. Lin, T. I., and Dowben, R. M. (1983) *J. Biol. Chem. 258*, 5142−5150.
42. Geeves, M. A., and Lehrer, S. S. (1994) *Biophys. J. 67*, 273−282.
43. Lehrer, S. S., Golitsina, N. L., and Geeves, M. A. (1997) *Biochemistry 36*, 13449−13454.
44. Margossian, S. S., and Cohen, C. (1982) *Methods Enzymol. 85*, 55−71.
45. Knight, P. J., and Trinnick, J.a. (1982) *Methods Enzymol. 85*, 9−12.
46. Nermut, M. V., and Eason, P. (1989) *Scanning Microsc.* (Suppl. 3), 213−224.
47. Domanus, J., Strambini, G. B., and Galley, W. C. (1980) *Photochem. Photobiol. 31*, 15−21.
48. Strambini, G. B., and Lehrer, S. S. (1991) *Eur. J. Biochem. 195*, 645−651.
49. Gekko, K., and Timasheff, S. N. (1981) *Biochemistry 20*, 4667−4676.
50. Gekko, I., and Ito, H. (1990) *J. Biochem. 107*, 572−577.
51. Timasheff, S. N., and Arawaka, T. (1989) in *Protein Structure: A Practical Approach* (Creighton, T. E., Ed.) pp 331−345, IRL Press, Oxford.
52. Eaton, B. L. (1976) *Science 192*, 1337−1339.

BI983073S